Self-supported NiMo hollow nanorod array: An efficient 3D bifunctional catalytic electrode for overall water splitting

ARTICLE *in* JOURNAL OF MATERIALS CHEMISTRY A · JANUARY 2015

Impact Factor: 7.44 · DOI: 10.1039/C5TA04723D

Journal of Materials Chemistry A

COMMUNICATION

View Article Online
View Journal | View Issue

Cite this: J. Mater. Chem. A, 2015, 3, 20056

Received 26th June 2015
Accepted 25th August 2015

DOI: 10.1039/c5ta04723d

www.rsc.org/MaterialsA

Self-supported NiMo hollow nanorod array: an efficient 3D bifunctional catalytic electrode for overall water splitting†

Jingqi Tian,[a] Ningyan Cheng,[a] Qian Liu,[a] Xuping Sun,*[a] Yuquan He*[b] and Abdullah M. Asiri[c]

Large-scale industrial application of electrochemical water splitting calls for remarkable non-noble metal electrocatalysts. Herein, we report on the synthesis of a NiMo-alloy hollow nanorod array supported on Ti mesh (NiMo HNRs/TiM) using a template-assisted electrodeposition method. The NiMo HNRs/TiM behaves as a durable efficient oxygen evolution anode with 10 mA cm^{-2} at an overpotential of 310 mV in 1.0 M KOH. Coupled with its superior catalytic performance for hydrogen evolution with 10 mA cm^{-2} at an overpotential of 92 mV, we made an alkaline electrolyzer using this bifunctional electrode with 10 mA cm^{-2} at a cell voltage of 1.64 V.

With the ever increasing energy crisis, substantial research efforts have been devoted to the development of clean energy. Hydrogen is considered as one of the most promising candidates for replacing fossil fuel-based energy.[1,2] As a well-established commercial technology for energy conversion, electrochemical water splitting offers a simple and promising path for hydrogen production.[3–5] The two half reactions of water splitting, hydrogen evolution reaction (HER) and oxygen evolution reaction (OER), both are crucial for the overall efficiency. The typical operating cell voltage for commercial electrolyzers (1.8–2.0 V), which is larger than the theoretical minimum value (~1.23 V), has a direct relationship with energy consumption and electrical efficiency.[6] The implementation of efficient electrocatalysts leads to decreased overpotentials, thereby making the whole process less energy-intensive.[7] The most efficient catalysts for HER (Pt-group metals[8]) and OER (Ru- and Ir-based compounds[9]) however suffer from scarcity and high price. It is therefore highly attractive to explore earth-abundant materials to overcome this obstacle.

Ni has emerged as an important non-noble metal due to its catalytic power for water splitting and Ni-based compounds have been intensively studied as efficient OER[10–15] and HER[16–29] catalysts. Water electrolysis must be performed in either strongly acidic or alkaline solution to minimize the overpotentials,[30] and the use of a bifunctional HER and OER catalyst can simplify the system and lower the cost. Alkaline water splitting has already found commercial applications for mass production of hydrogen.[6] Accordingly, it is highly desired to develop bifunctional OER and HER catalysts operating efficiently in basic electrolytes, but only very limited success has been achieved in making Ni-based ones so far, including $Ni(OH)_2$/NF and NiFe LDH/NF,[31] Ni_2P/NF,[32] and NiSe/NF.[33]

Herein, we describe a template-assisted electrodeposition route to synthesize a NiMo-alloy hollow nanorod array supported on Ti mesh (NiMo HNRs/TiM). When used as a 3D oxygen evolution catalytic anode, such NiMo HNRs/TiM requires an overpotential of only 310 mV to obtain 10 mA cm^{-2} with strong durability in 1.0 M KOH. As a hydrogen evolution cathode, this electrode achieves 10 mA cm^{-2} at an overpotential of only 92 mV in the same electrolyte. Notably, the alkaline water electrolyzer using the NiMo HNRs/TiM as both anode and cathode affords 10 mA cm^{-2} water-splitting current at a cell voltage of 1.64 V.

A ZnO nanorod array grown on TiM (ZnO NRs/TiM)[34] was used as a template for Ni–Mo electrodeposition. Fig. 1A shows the low-magnification scanning electron microscopy (SEM) image, indicating that the entire surface of the TiM (Fig. S1A†) was uniformly coated with ZnO nanorods. The high-magnification SEM image (inset) further reveals that the ZnO nanorods have diameters of 200–500 nm. After the electrodeposition of Ni–Mo, the nanorods preserve their 1D morphology with an enlarged diameter of 400–600 nm (Fig. 1B), suggesting that the Ni–Mo layer was preferentially deposited on the surface to the interspaces of the ZnO nanorods. Removing the ZnO template leads to the NiMo hollow nanorod array supported on the TiM (NiMo

[a]State Key Laboratory of Electroanalytical Chemistry, Changchun Institute of Applied Chemistry, Chinese Academy of Sciences, Changchun 130022, Jilin, China. E-mail: sunxp@ciac.jl.cn; Fax: +86-431-85262065; Tel: +86-431-85262065

[b]Department of Cardiology, China-Japan Union Hospital of Jilin University, Changchun 130033, China. E-mail: yuquanhe@hotmail.com

[c]Chemistry Department, Faculty of Science, King Abdulaziz University, Jeddah, 21589, Saudi Arabia

† Electronic supplementary information (ESI) available: Experimental section and supplementary figures and table. See DOI: 10.1039/c5ta04723d

HNRs/TiM), as shown in Fig. 1C and Fig. S1B.† Fig. S2† shows the energy-dispersive X-ray (EDX) spectra of these three samples. Fig. 1D shows the X-ray diffraction (XRD) pattern of such NiMo hollow nanorods scratched from TiM, and all diffraction peaks correspond to the Ni_4Mo phase (JCPDS no. 65-5480).[26] The EDX spectrum also verifies the 4 : 1 atomic ratio between Ni and Mo (Fig. S2†). The composition of scratched NiMo hollow nanorods was further analyzed by inductively coupled plasma optical emission spectrometry (ICP-OES), suggesting a molar ratio of 4 : 1.01 between Ni and Mo, which is consistent with the EDX results. The transmission electron microscopy (TEM) images reveal that such NiMo hollow nanorods have an average diameter of 500 nm, which is composed of intercrossed nanosheets to create loose porous nanostructures (Fig. 1E and F). The high-resolution TEM (HRTEM) image (Fig. 1G) shows that the NiMo hollow nanorod has clear lattice fringes with an interplanar distance of 0.201 nm corresponding to the (220) plane of Ni_4Mo.[26] Fig. 1H shows the scanning TEM (STEM) image and the corresponding EDX elemental mapping images of Ni and Mo of the NiMo hollow nanorod, indicating that both Ni and Mo elements are uniformly distributed in the hollow nanorod. It is important to mention that electrodeposition of Ni–Mo on bare TiM without the ZnO template leads to Ni–Mo nanoparticle film coated TiM (NiMo NPs/TiM), as shown in Fig. S3.†

Fig. 2A shows polarization curves of NiMo HNRs/TiM (NiMo loading: 0.68 mg cm^{-2}) in 1.0 M KOH with a scan rate of 2 mV s^{-1}. All the data were recorded in a standard three-electrode electrochemical cell. Because the as-measured reaction currents cannot reflect the intrinsic behaviour of electrocatalysts due to the effect of ohmic resistance, resistance tests were made for iR correction of all initial data for further analysis.[35] For a comparative study, we also tested NiMo NPs/TiM and RuO_2 loaded on TiM (RuO_2/TiM). NiMo HNRs/TiM is significantly active for the OER with an onset potential as low as 1.53 V *vs.* the reversible hydrogen electrode (RHE), and more rapid increase in current is observed at higher potentials. Note that NiMo NPs/TiM also functions as an OER anode but with a much larger onset potential (1.58 V). Moreover, the NiMo HNRs/TiM affords 10 mA cm^{-2} at an overpotential (η_{OER}) of 310 mV, which is much smaller than that of NiMo NPs/TiM (350 mV). This overpotential compares favourably with the behaviour of Ni-based OER electrocatalysts except the Ni + Mo composite (Table S1†). Although RuO_2/TiM affords a lower onset potential (1.48 V) and η_{OER} (260 mV), its OER current density drops below that of NiMo HNRs/TiM in the potential region higher than 1.59 V. The Tafel slope for NiMo HNRs/TiM is 47 mV dec^{-1}, which is lower than that of NiMo NPs/TiM (68 mV dec^{-1}) and RuO_2/TiM (62 mV dec^{-1}), as shown in Fig. 2B, suggesting the favourable reaction kinetics for NiMo HNRs/TiM.

It is reported that the increment of electrocatalytic activity may arise from increasing surface area of the catalyst with different morphologies.[36,37] To estimate the active surface area of NiMo HNRs/TiM and NiMo NPs/TiM, we measured the electrochemical double-layer capacitance (C_{dl}) at the solid/liquid interface of both electrodes.[38] The cyclic voltammograms (CVs) were measured in the region of 0.08–0.18 V, where the current response should only be due to the charging of the double layer (Fig. S4A and S4B†). The values of C_{dl} for NiMo HNRs/TiM and NiMo NPs/TiM are 3.56 and 0.66 mF cm^{-2}, respectively. Since C_{dl} is proportional to the active surface area of the electrocatalysts, the result suggests that NiMo HNRs/TiM possesses a larger active surface area compared with NiMo NPs/TiM. Thus, we possibly attribute the superior catalytic activity of NiMo HNRs/TiM over NiMo NPs/TiM to its higher surface area.

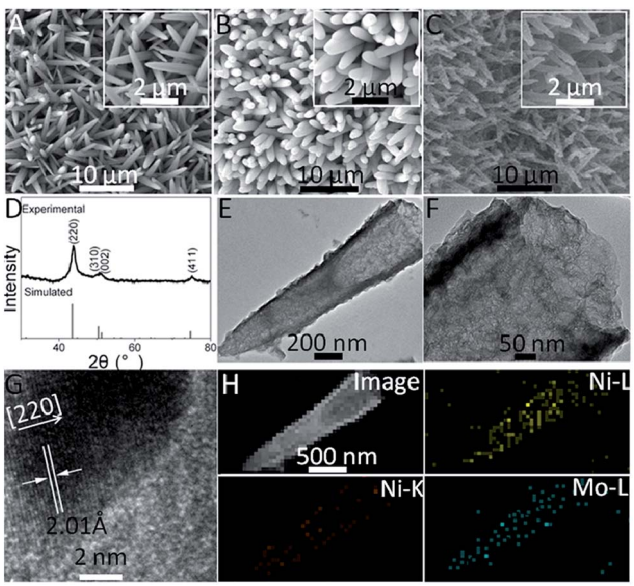

Fig. 1 SEM images of (A) ZnO NRs/TiM, (B) ZnO@NiMo NRs/TiM, and (C) NiMo HNRs/TiM. (D) XRD pattern of NiMo-alloy hollow nanorods. (E and F) TEM images of one single NiMo-alloy hollow nanorod. (G) HRTEM image taken from the NiMo-alloy hollow nanorod. (H) STEM image and the corresponding EDX elemental mapping images of Ni and Mo for one single NiMo-alloy hollow nanorod.

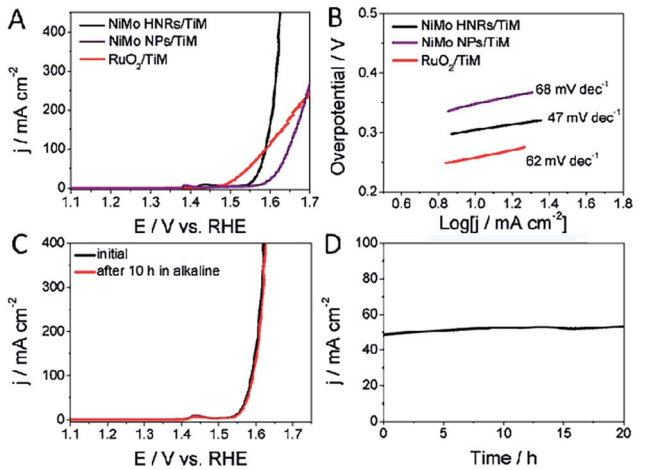

Fig. 2 (A) Polarization curves of NiMo HNRs/TiM, NiMo NPs/TiM and RuO_2/TiM with a scan rate of 2 mV s^{-1} in 1.0 M KOH. (B) The corresponding Tafel plots. (C) Polarization curves of NiMo HNRs/TiM initially and after chronopotentiometric electrolysis of 10 h. (D) Time-dependent current density curve of NiMo HNRs/TiM under a static overpotential of 350 mV for 20 h.

We also examined the durability of NiMo HNRs/TiM for OER. As shown in Fig. 2C, the NiMo HNRs/TiM maintains its full OER activity after chronopotentiometric electrolysis of 10 h in 1.0 M KOH. The electrochemical stability of the NiMo HNR/TiM electrode was tested in bulk electrolysis of water, as shown in Fig. 2D. NiMo HNRs/TiM delivers a current density of 50 mA cm^{-2} under a static overpotential of 350 mV, and stabilizes around this value during the 20 h electrolysis with small change in current density (~4 mA cm^{-2}).

The electrochemical HER activity of the NiMo HNRs/TiM, NiMo NPs/TiM, and Pt/C on TiM (Pt/C/TiM) was also evaluated in 1.0 M KOH. Fig. 3A shows the polarization curves with iR compensation. Pt/C/TiM shows a negligible onset overpotential, which is 60 and 125 mV for NiMo HNRs/TiM and NiMo NPs/TiM, respectively. NiMo HNRs/TiM requires the overpotential (η_{HER}) of 92 mV to achieve 10 mA cm^{-2}, which compares favorably with the behavior of most reported HER catalysts listed in Table S2.† Note that Mo HNRs/TiM needs an η of 200 mV to achieve 100 mA cm^{-2}, which is much smaller than that of Pt/C/TiM (265 mV) and NiMo NPs/TiM (275 mV), implying the superior HER activity of the NiMo HNR/TiM electrode. As shown in Fig. 3B, the Tafel slope for Pt/C/TiM, NiMo HNRs/TiM, and NiMo NPs/TiM is 31, 76, and 94 mV dec^{-1}, respectively. We also examined the durability of the NiMo HNRs/TiM for the HER. The polarization curve shows a negligible difference compared with the initial one after continuous CV scanning for 1000 cycles (Fig. 3C). The long-term electrochemical stability of this electrode was further tested in bulk electrolysis of water. Fig. 3D presents the time-dependent current density curve under a static overpotential of 140 mV, suggesting that NiMo HNRs/TiM maintains its catalytic activity for at least 15 h. All these results demonstrate the excellent activity and stability of the NiMo NP/TiM electrode for the HER in 1.0 M KOH.

Based on the results that NiMo HNRs/TiM is efficient for both OER and HER in basic media, we demonstrate the capability of utilizing the NiMo HNRs/TiM as both anode and cathode to construct a water splitting electrolyzer. As shown in Fig. 4A, this electrolyzer can achieve 10 mA cm^{-2} at a cell voltage of 1.64 V in 1.0 M KOH, which is much smaller than that of the electrolyzer using NiMo NPs/TiM as both electrodes (NiMo NPs/TiM||NiMo NPs/TiM, 1.70 V) although 70 mV is larger than that of the electrolyzer using RuO_2/TiM and Pt/C/TiM as the anode and cathode (RuO_2/TiM||Pt/C/TiM). This voltage is much smaller than that needed by $Ni(OH)_2$/NF||$Ni(OH)_2$/NF (~1.82 V) and NiFe LDH/NF||NiFe LDH/NF (1.7 V)[31] and even comparable to that needed by Ni_2P/NF||Ni_2P/NF (1.63 V)[32] and NiSe/NF||NiSe/NF (1.63 V).[33] When the applied voltage is set at 1.64 V, a constant current density of 10 mA cm^{-2} can be well maintained for 10 h, as shown in Fig. 4B. It is worth mentioning that efficient water electrolysis can be powered by a single-cell AAA battery with a nominal voltage of ~1.5 V (Fig. 4C and Movie S1†). These results indicate that our NiMo HNR/TiM electrode holds great promise for practical alkaline water electrolysis applications.

In summary, the NiMo-alloy hollow nanorod array has been developed successfully on Ti mesh using a template-assisted electrodeposition method. Such NiMo HNRs/TiM behaves as a highly efficient and durable bifunctional catalytic electrode for both OER and HER in alkaline media, enabling the construction of a stable two-electrode alkaline water electrolyzer with 10 mA cm^{-2} water-splitting current at a cell voltage of 1.64 V. Our present study is important for the following three reasons: (1) it is the first demonstration of the NiMo-alloy hollow nanorod array as a self-supported bifunctional electrode toward water splitting with high catalytic activity and stability; (2) it presents

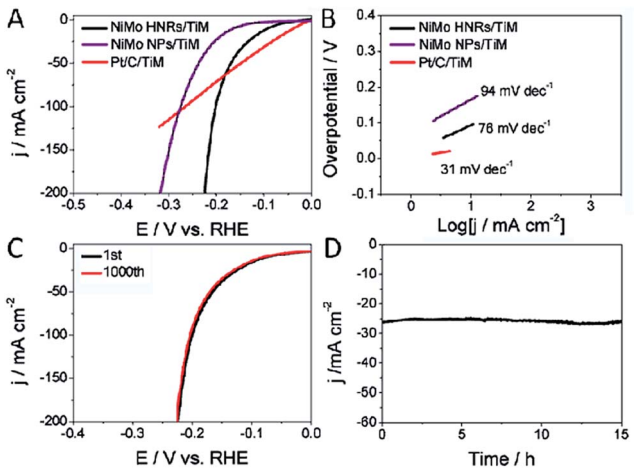

Fig. 3 (A) Polarization curves of NiMo HNRs/TiM, NiMo NPs/TiM, and Pt/C/TiM with a scan rate of 2 mV s^{-1} in 1.0 M KOH. (B) The corresponding Tafel plots. (C) Polarization curves of NiMo HNRs/TiM initially and after 1000 CV scanning between +0.1 and −0.2 V *vs.* RHE. (D) Time-dependent current density curve of NiMo HNRs/TiM under a static overpotential of 140 mV for 15 h.

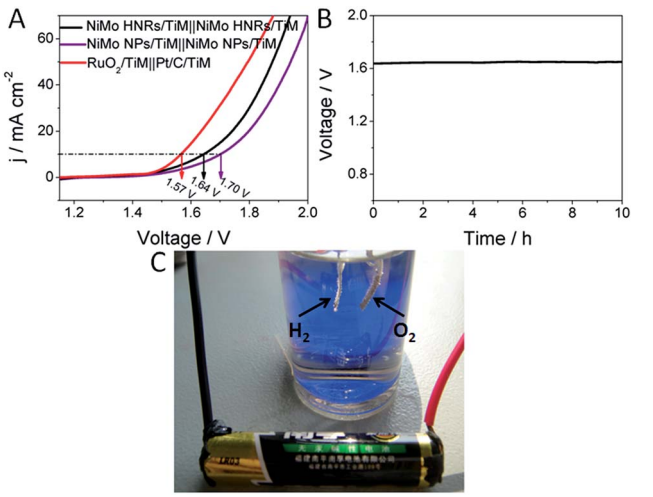

Fig. 4 (A) Polarization curves of water electrolysis for NiMo HNRs/TiM||NiMo HNRs/TiM, NiMo NPs/TiM||NiMo NPs/TiM, and RuO_2/TiM||Pt/C/TiM with a scan rate of 2 mV s^{-1} in 1.0 M KOH. (B) Chronopotentiometric curve of water electrolysis for NiMo HNRs/TiM||NiMo HNRs/TiM with a constant current density of 10 mA cm^{-2}. (C) The NiMo HNRs/TiM||NiMo HNRs/TiM water splitting system driven by an ~1.5 V AAA battery.

a facile and scale-up fabrication strategy for the development of water splitting catalysts; (3) it highlights the potential of the NiMo-alloy hollow nanorod array as an attractive catalyst in large-scale production of hydrogen fuel application, opening an exciting new avenue to explore the use of non-precious and environmentally friendly metal alloys in future water splitting devices.

Acknowledgements

This work was supported by the National Natural Science Foundation of China (no. 21175129) and the National Basic Research Program of China (no. 2011CB935800).

Notes and references

1 R. F. Service, *Science*, 2004, **305**, 958.
2 K. S. Joya, Y. F. Joya, K. Ocakoglu and R. Krol, *Angew. Chem., Int. Ed.*, 2013, **52**, 10426.
3 J. A. Turner, *Science*, 2004, **305**, 972.
4 C. S. Lim, Z. Sofer, R. J. Toh, A. Y. S. Eng, J. Luxa and M. Pumera, *ChemPhysChem*, 2015, **16**, 1898.
5 F. M. Toma, A. Sartorel, M. Iurlo, M. Carraro, S. Rapino, L. Hoober-Burkhardt, T. Ros, M. Marcaccio, G. Scorrano, F. Paolucci, M. Bonchio and M. Prato, *ChemSusChem*, 2011, **4**, 1447.
6 K. Zeng and D. Zhang, *Prog. Energy Combust. Sci.*, 2010, **36**, 307.
7 M. G. Walter, E. L. Warren, J. R. McKone, S. W. Boettcher, Q. Mi, E. A. Santori and N. S. Lewis, *Chem. Rev.*, 2010, **110**, 6446.
8 J. Tian, Q. Liu, A. M. Asiri and X. Sun, *J. Am. Chem. Soc.*, 2014, **136**, 7587.
9 Y. Lee, J. Suntivich, K. J. May, E. E. Perry and Y. Shao-Horn, *J. Phys. Chem. Lett.*, 2012, **3**, 399.
10 S. Chen, J. Duan, M. Jaroniec and S. Qiao, *Angew. Chem., Int. Ed.*, 2013, **52**, 13567.
11 D. Friebel, M. W. Louie, M. Bajdich, K. E. Sanwald, Y. Cai, A. M. Wise, M. J. Cheng, D. Sokaras, T. C. Weng, R. Alonso-Mori, R. C. Davis, J. R. Bargar, J. K. Nørskov, A. Nilsson and A. T. Bell, *J. Am. Chem. Soc.*, 2015, **137**, 1305.
12 R. D. L. Smith, M. S. Prévot, R. D. Fagan, Z. Zhang, P. A. Sedach, M. K. Siu, S. Trudel and C. P. Berlinguette, *Science*, 2013, **340**, 60.
13 M. Dinca, Y. Surendranath and D. G. Nocera, *Proc. Natl. Acad. Sci. U. S. A.*, 2010, **107**, 10337.
14 M. Ledendecker, G. Clavel, M. Antonietti and M. Shalom, *Adv. Funct. Mater.*, 2015, **25**, 393.
15 L. Xiao, S. Zhang, J. Pan, C. Yang, M. He, L. Zhuang and J. Lu, *Energy Environ. Sci.*, 2012, **5**, 7869.
16 M. Gong, W. Zhou, M.-C. Tsai, J. Zhou, M. Guan, M.-C. Lin, B. Zhang, Y. Hu, D.-Y. Wang, J. Yang, S. J. Pennycook, B.-J. Hwang and H. Dai, *Nat. Commun.*, 2014, **5**, 4695.
17 M. S. Faber and S. Jin, *Energy Environ. Sci.*, 2014, **7**, 3519.
18 N. Jiang, L. Bogoev, M. Popova, S. Gul, J. Yano and Y. Sun, *J. Mater. Chem. A*, 2014, **2**, 19407.
19 P. Jiang, Q. Liu and X. Sun, *Nanoscale*, 2014, **6**, 13440.
20 Z. Pu, Q. Liu, C. Tang, A. M. Asiri and X. Sun, *Nanoscale*, 2014, **6**, 11031.
21 E. J. Popczun, J. R. McKone, C. G. Read, A. J. Biacchi, A. M. Wiltrout, N. S. Lewis and R. E. Schaak, *J. Am. Chem. Soc.*, 2013, **135**, 9267.
22 L. Feng, H. Vrubel, M. Bensimon and X. Hu, *Phys. Chem. Chem. Phys.*, 2014, **16**, 5917.
23 W.-F. Chen, K. Sasaki, C. Ma, A. I. Frenkel, N. Marinkovic, J. T. Muckerman, Y. Zhu and R. R. Adzic, *Angew. Chem., Int. Ed.*, 2012, **51**, 6131.
24 J. R. McKone, B. F. Sadtler, C. A. Werlang, N. S. Lewis and H. B. Gray, *ACS Catal.*, 2013, **3**, 166.
25 D. E. Brown, M. N. Mahmood, A. K. Turner, S. M. Hall and P. O. Fogarty, *Int. J. Hydrogen Energy*, 1982, **7**, 405.
26 Y. Wang, G. Zhang, W. Xu, P. Wan, Z. Lu, Y. Li and X. Sun, *ChemElectroChem*, 2014, **1**, 1138.
27 J. R. McKone, E. L. Warren, M. J. Bierman, S. W. Boettcher, B. S. Brunschwig, N. S. Lewis and H. B. Gray, *Energy Environ. Sci.*, 2011, **4**, 3573.
28 C. Tang, Z. Pu, Q. Liu, A. M. Asiri and X. Sun, *Electrochim. Acta*, 2015, **153**, 508.
29 C. Tang, Z. Pu, Q. Liu, A. M. Asiri, Y. Luo and X. Sun, *Int. J. Hydrogen Energy*, 2015, **40**, 4727.
30 E. A. Hernández-Pagán, N. M. Vargas-Barbosa, T. H. Wang, Y. Zhao, E. S. Smotkin and T. E. Mallouk, *Energy Environ. Sci.*, 2012, **5**, 7582.
31 J. Luo, J.-H. Im, M. T. Mayer, M. Schreier, M. K. Nazeeruddin, N. G. Park, S. D. Tilley, H. Fan and M. Grätzel, *Science*, 2014, **345**, 1593.
32 L.-A. Stern, L. Feng, F. Song and X. Hu, *Energy Environ. Sci.*, 2015, **8**, 2347–2351.
33 C. Tang, N. Cheng, Z. Pu, W. Xing and X. Sun, *Angew. Chem., Int. Ed.*, 2015, **54**, 9351.
34 Z. Xing, Q. Chu, X. Ren, C. Ge, A. H. Qusti, A. M. Asiri, A. O. Al-Youbi and X. Sun, *J. Power Source*, 2014, **245**, 463.
35 Z. Xing, Q. Liu, A. M. Asiri and X. Sun, *Adv. Mater.*, 2014, **26**, 5702.
36 J. Xie, S. Li, X. Zhang, J. Zhang, R. Wang, H. Zhang, B. Pan and Y. Xie, *Chem. Sci.*, 2014, **5**, 4615.
37 M. A. Lukowski, A. S. Daniel, F. Meng, A. Forticaux, L. Li and S. Jin, *J. Am. Chem. Soc.*, 2013, **135**, 10274.
38 J. Tian, Q. Liu, N. Cheng, A. M. Asiri and X. Sun, *Angew. Chem., Int. Ed.*, 2014, **53**, 9577.